Supplementary Information for

Data driven pilot optimization for the electrochemical CO mass production

Kyeongsu Kim[a], WoongHee Lee[a], Jonggeol Na[d], YunJeong Hwang[a], Hyeong-suk Oh[a*] and Ung Lee[a, b, c*]

[a] Clean Energy Research Center, Korea Institute of Science and Technology, Seoul 02792, Republic of Korea

[b] Division of Energy & Environment Technology, KIST school, Korea University of Science and Technology, Seoul 02792, Republic of Korea

[c] Green School, Korea University, Seoul 151-742, South Korea

[d] Division of Chemical Engineering and Materials Science, Ewha Womans University, Seoul 03760, Republic of Korea

2020. 06.01

*Author to whom correspondence should be addressed.

Tel.: 82-2-958-5812 E-mail: ulee@kist.re.kr

Supplementary Information.

Gaussian Process Bayesian Optimization.

The Gaussian process Bayesian optimization (GPBO) algorithm can be used to address optimization problems of which objective function is expansive by predicting the experimental results using input-output relations, which in turn leads us to avoid performing unnecessary experiments. Here, we use the Thompson sampling Bayesian optimization with the hyperparameters of its kernel function estimated using maximum a posteriori (MAP)[1]. The algorithm is modified to be suitable for optimization of the pilot-scale CO production system. When assuming the evaluations of j_{CO} is distributed as a Gaussian Process (GP) with its zero mean function and covariance function, $k(x, x')$, then it can be expressed as:

$$j_{CO}(x) \sim GP(0, k(x,x')) \quad \text{(S1)}$$

where the operating condition, $x = \{E, \text{T}, \text{P}\}$, is the vector of optimization variables. Note that the acquisition function, $\alpha(x)$, for GPBO is selected as the surrogate model describing $j_{CO}(x)$. The covariance function, $k(x,x')$, is commonly selected from the stationary Matérn class. In this study, Matérn 3 kernel is adopted to approximate the covariance function[2]

$$k(x,x') = \sigma_\alpha^2(1+\sqrt{3}r)\exp(-\sqrt{3}r) + \sigma_n^2\delta(x,x') \quad \text{(S2)}$$

where σ_α is the output variance of $\alpha(x)$, σ_n is the observation noise, and δ is the Kronecker delta. The distance, r, can be calculated as:

$$r = \sqrt{(x-x')\Lambda(x-x')} \quad \text{(S3)}$$

where Λ is diagonal matrix of which elements indicate the length scales of the optimization variables. The GP can be defined using the hyperparameters, $\{\sigma_\alpha, \sigma_n, \Lambda\}$, and

each of them is assumed to follow a normal distribution. MAP estimator is adopted to find the best estimate of the hyperparameters using training data[1]. When n_t number of training points, $X = \{x_1, \ldots, x_{n_t}\}$, and their corresponding evaluations of the CO partial current density, $Y = \{j_{CO}(x_1), \ldots, j_{CO}(x_{n_t})\} = \{y_1, \ldots, y_{n_t}\}$, are given, the covariance function of the posterior distribution resulted from MAP estimation can be derived as in Eq. (S4).

$$k(x,x')|X,Y = k(x,x') - \Sigma(x,X)\Sigma^{-1}\Sigma(x,X)^T \quad \text{(S4)}$$

where $\Sigma = |k(x,x')|_{n_t \times n_t}$, and $\Sigma(x,X) = |k(x,x_1'), \ldots, k(x,x_{n_t}')|$.

The covariance function can be approximated as $k(x,x') = \xi(x)^T\xi(x)$, and using spectral sampling, the multiplicand, $\xi(x)$, is described as:

$$\xi(x) = \sqrt{2\frac{\beta}{M}}cos(Wx + b) \quad \text{(S5)}$$

where $\beta = \sigma_\alpha^2$ is a proportionality constant and M is the number of samples. W and b are sampled from the probability distribution of the hyperparameters and the uniform distribution, $U(0, 2\pi)$, respectively. The acquisition function is known to be linearly approximated using $\xi(x)$.

$$\alpha(x) \approx \xi(x)^T\theta \quad \text{(S6)}$$

where $\theta \sim N(m, V)$. The values of m and V are derived as:

$$m = \left(Z^TZ + \sigma_n^2 I\right)^{-1}Z^TY^{-1} \quad \text{(S7)}$$

$$V = \left(Z^TZ + \sigma_n^2 I\right)^{-1}\sigma_n^2 \quad \text{(S8)}$$

where Z indicates the collection of $\xi(x)$ estimated at $X = \{x_1, \ldots, x_{n_t}\}$. The k^{th} acquisition function sampled from the posterior distribution of the hyperparameter is given by:

$$\alpha_k(x) \approx \xi_k(x)^T \theta_k \tag{S9}$$

where $\theta_k \sim N(m_k, V_k)$. The $(k+1)^{th}$ evaluation point is obtained by performing minimization of the acquisition function Eq. (S11).

$$x_{k+1} = argmin_x \, \alpha_k(x) \tag{S10}$$

Eq. (S12) is solved using Genetic Algorithm (GA)[3].

Computer-aided design of in-house single cell with pin-type channels.

To design the optimal electrochemical single cell pin structure of both cathode and anode side for electrolyte stream, we employed finite-volume methods (FVM) based computational fluid dynamics (CFD) model. Two-layered fluid zones consisted of electrolyte flow zone and porous zone (carbon paper with a catalyst with porosity 0.73) was used to represent in-house single cell with pin-type channels under convective mass transfer of CO_2 saturated aqueous electrolyte solution (Fig. S1). Three-dimensional Navier-Stokes equation with the k-epsilon turbulence model was used. Notably, carbon paper with a catalyst for electrochemical CO_2 reduction reaction was assumed as porous media so that mass transport through convection can be detected forced by pressure differences. Simulations were performed by using ANSYS FLUENT 18.2 with MPI parallel computing using four cores of Intel i7-7820X (3.6 GHz) processors.

We carried out the comparative study between two geometry cases (case 1: 1 mm / 1mm) and (case 2: 4.3 mm / 4.5 mm) of (fin width and fin distance), respectively (Fig. S2). Through the simulation results, we can infer that the fin distance and width should be narrow, which can improve the overall cell performance. This is because the narrower the fin distance and the width increase the pressure drop (Fig. S3), which leads to developing the velocity vector field of electrolyte with aqueous CO_2 moving toward the carbon paper (Fig. S2 (c) and (d)). Thus, this acceleration of mass transport can increase the CO_2 concentration at the catalyst layer, which leads to an increase in current density and CO Faraday efficiency.

In order to analyze reactor performance more quantitatively, global sensitivity analysis of pressure drop (ΔP), velocity uniformity (γ_a),), and average velocity ($\bar{v}_a$) for fin width and fin distance was performed (Fig. S4). Pressure drop was calculated as the pressure

difference between inlet and outlet. Area-weighted velocity uniformity and area-weighted average velocity were defined by Eq. (S11) and Eq. (S12), respectively.

$$\gamma_a = 1 - \frac{\sum_{i=1}^{N} [(|v_i - \bar{v}_a|)A_i]}{2|\bar{v}_a| \sum_{i=1}^{N} A_i} \quad \text{(S11)}$$

$$\bar{v}_a = \frac{\sum_{i=1}^{N} v_i A_i}{\sum_{i=1}^{N} A_i} \quad \text{(S12)}$$

where v_i and A_i are velocity and area at index i on N facets. Therefore, γ_a has a value between 0 and 1, and the closer it is to 1, the more evenly distributed the entire surface, and $\bar{v}_a$ is the average value of the velocity at the specified surface. In order to maintain high reactivity, uniformity at porous media should be close to 1 because it is good to have a constant overall flow rate in a porous layer with a catalyst. In addition, slow average velocity is preferred in order to maximize the reactivity by securing a sufficient residence time (Fig. S4 (c), (d)). In order to satisfy this, it was confirmed that a relatively dense fin structure has more advantages because inevitably, high ΔP is required (Fig. S4 (b). Therefore, the design suggestion through the computer-aided design framework in this study is that fin width and fin distance should be designed between 1 mm – 2 mm. We fabricated the pin-type chanell cell for 50 cm^2 active area with 1.5 mm fin width and distance to perform this pilot plant study.

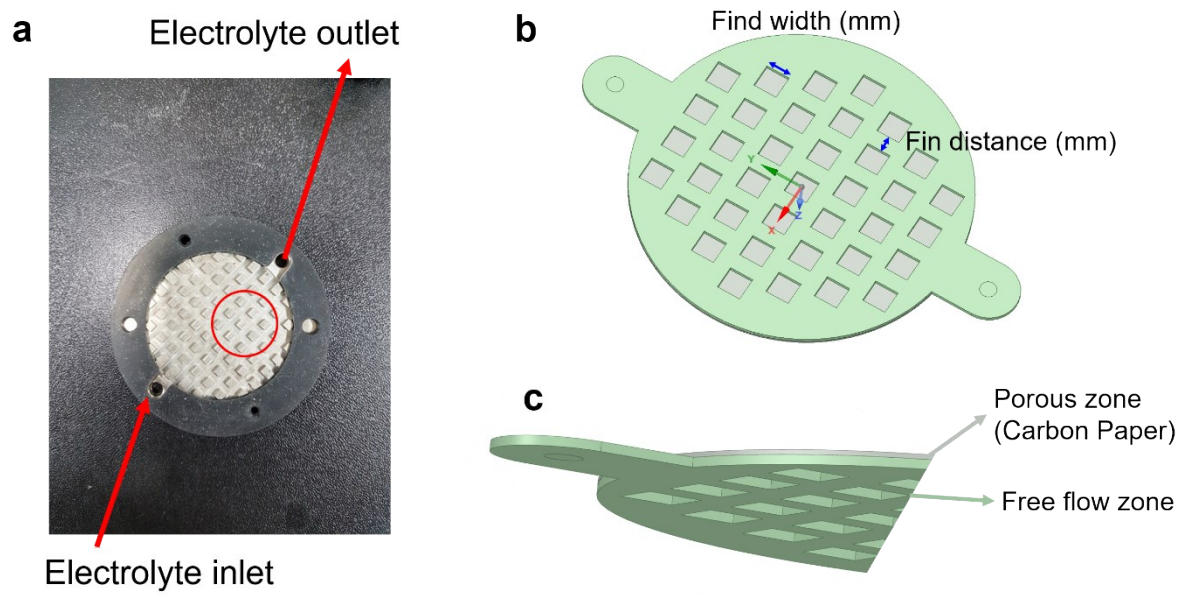

Figure S1. Computer-aided design for in-house single cell with pin-type channels. (a) The prototype fin structure with inlet and outlet channel. (b) Design variables (fin width and fin distance) to optimize the performance of the cell. (c) Side view geometry of simulation boundaries.

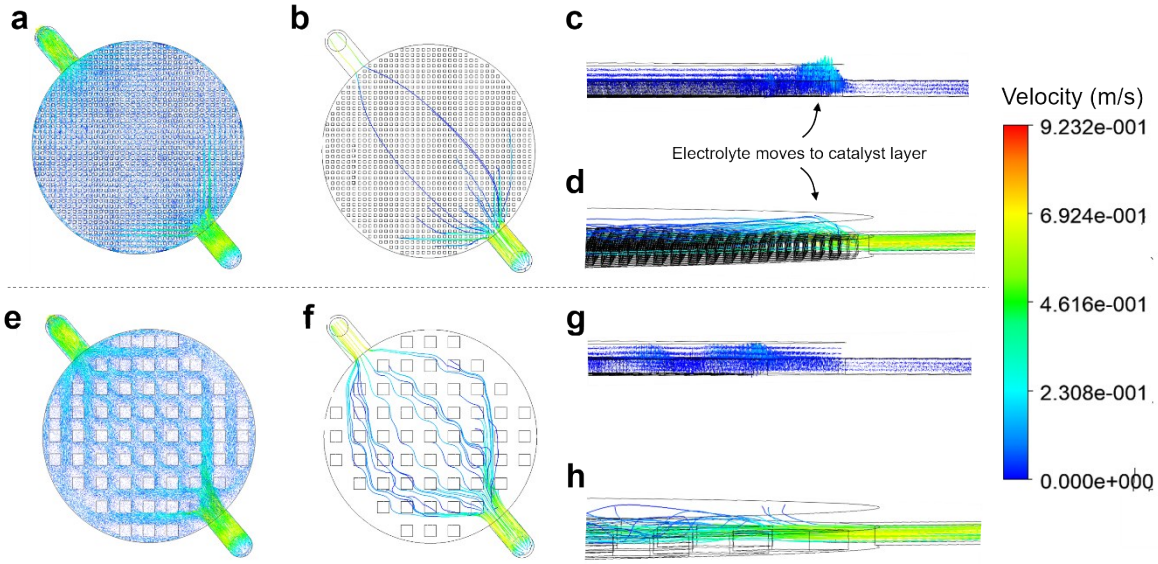

Figure S2. Comparison of velocity vector field and streamline in computational fluid dynamics simulation data of at different design variables of (a-d) fin width as 1 mm and fin distance as 1 mm, and (e-f) fin width as 4.34 mm and fin distance as 4.5 mm. (a,e) Velocity vector field at top view. (b,f) Streamline at top view. (c,g) Velocity vector field at side view. (d,h) Streamline at side view.

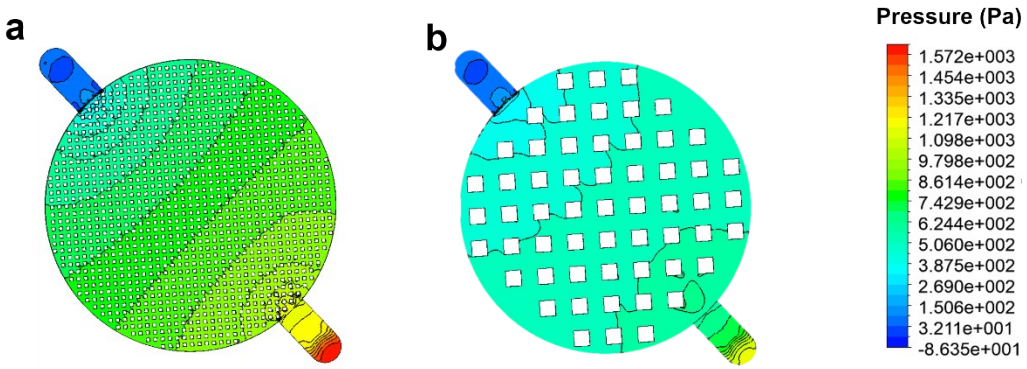

Figure S3. Pressure drop comparison at different design variables of (a) fin width as 1 mm and fin distance as 1 mm, and (b) fin width as 4.34 mm and fin distance as 4.5 mm. Black solid lines denotes equal pressure sections.

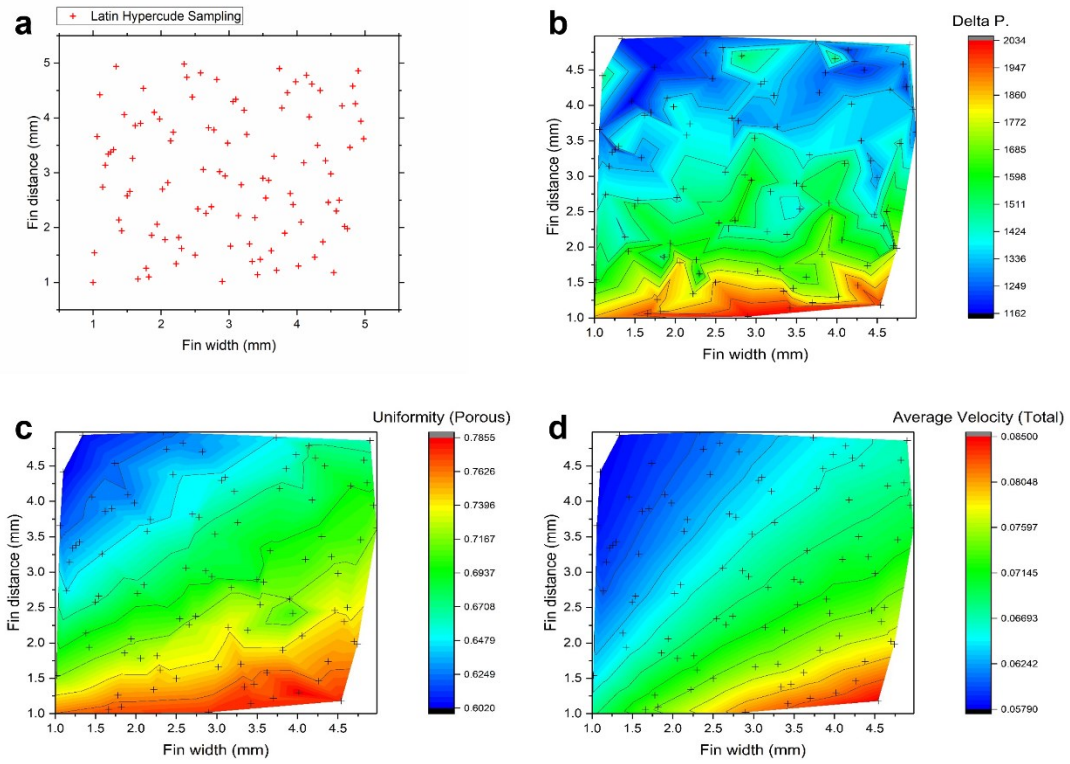

Figure S4. Results of global sensitivity analysis using Latin hypercube sampling (a) throughout global space of design variables. Two-dimensional contour plot of (b) pressure drop, (c) uniformity at porous zone, and (d) average velocity at total zone (porous zone + free flow zone).

Ag catalyst charactorization.

The Cl doping concentrations are measured through energy dispersive spectroscopy (EDS) spectra of scanning electron microscopy (SEM), as shown in Figure S5. The measured Cl doping concentration was 1.22%. The morphology of Cl doped Ag electrode was demonstrated by SEM and their results are shown in Figure S6. Their morphology has a porous structure, which is considered to be good for mass transfer of CO_2. In addition, the chemical state of the Ag electrode before and after Cl doping treatment, X-ray photoelectron spectroscopy (XPS) was conducted and their results are shown in Figure S7. After Cl doping process, Ag electrode was slightly oxidized owing to remained Cl component.

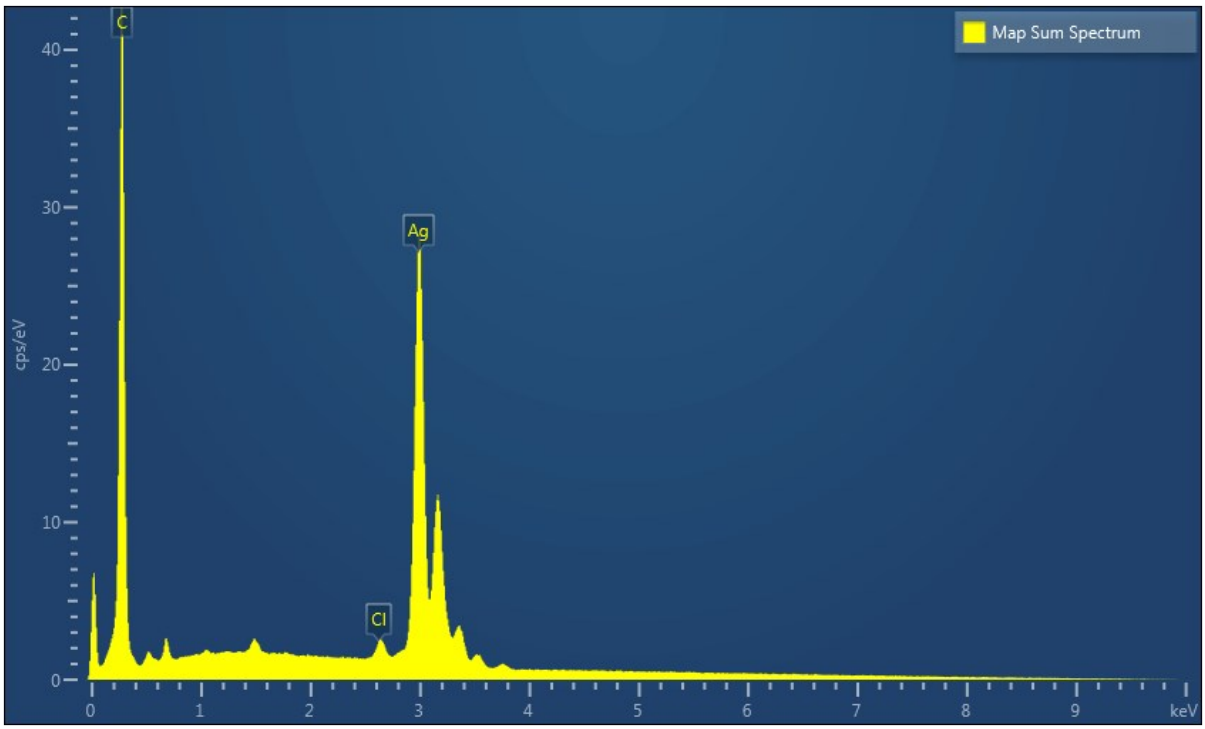

Figure S5. The EDS spectrum of Cl doped Ag electrode.

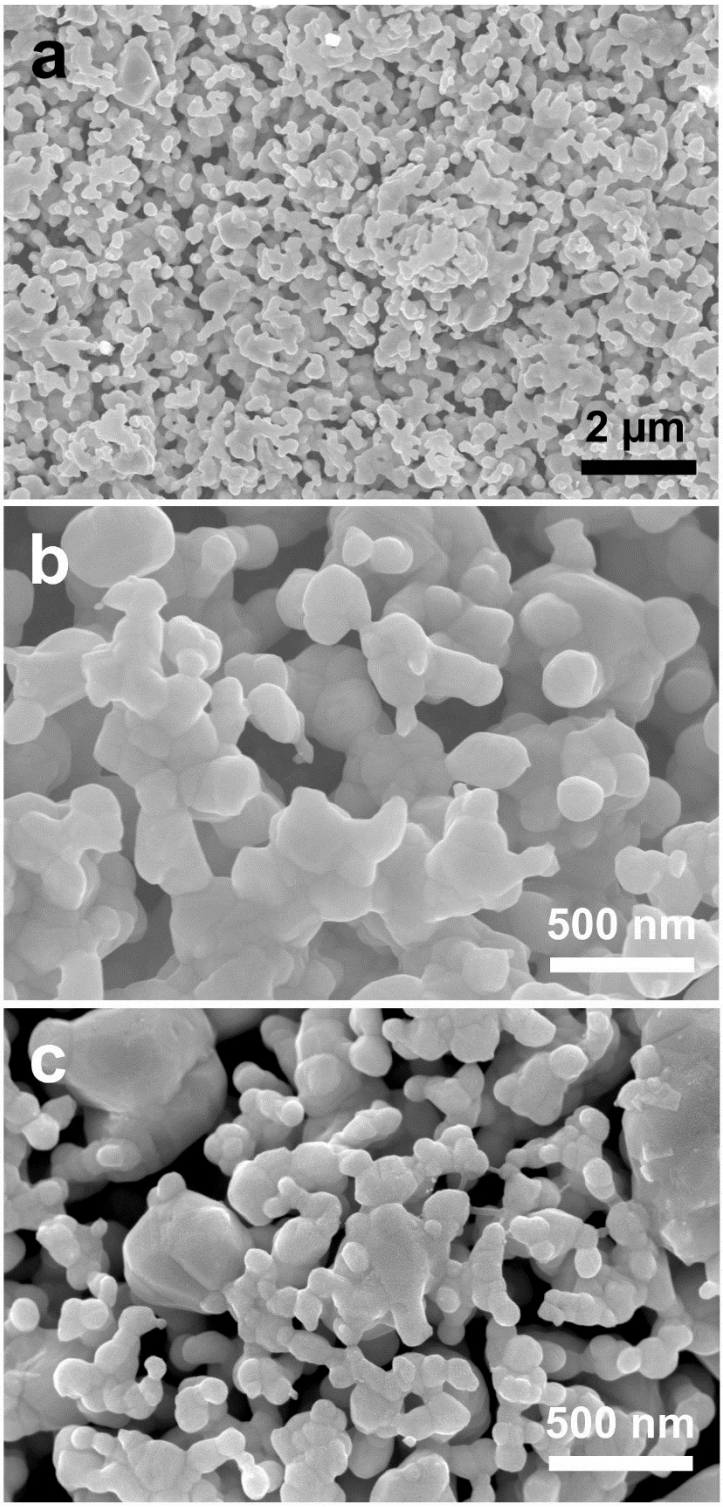

Figure S6. (a) Low and (b, c) high magnification SEM images of Cl doped Ag electrode.

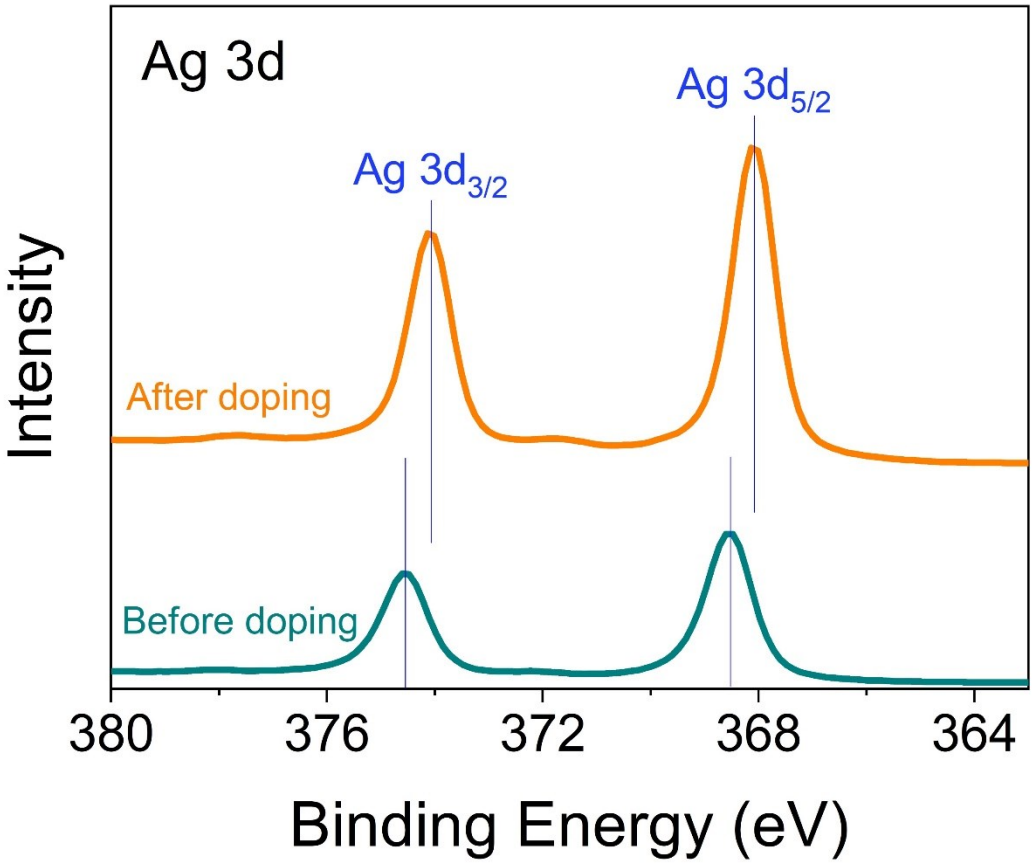

Figure S7. XPS spectra of the Ag 3d for Ag electrode before and after Cl doping process.

References

1. Bradford, E.; Schweidtmann, A. M.; Lapkin, A., Efficient multiobjective optimization employing Gaussian processes, spectral sampling and a genetic algorithm. *Journal of global optimization* **2018,** *71* (2), 407-438.

2. Genton, M. G., Classes of kernels for machine learning: a statistics perspective. *Journal of machine learning research* **2001,** *2* (Dec), 299-312.

3. Conn, A.; Gould, N.; Toint, P. J. M. o. C., A globally convergent Lagrangian barrier algorithm for optimization with general inequality constraints and simple bounds. *Mathematics of Computation* **1997,** *66* (217), 261-288.